Co-deposition of bismuth-nitrogen films on MgO (001) by molecular beam epitaxy

Ashok Shrestha, Ali Abbas, David C. Ingram, and Arthur R. Smith*

Nanoscale and Quantum Phenomena Institute,

Department of Physics and Astronomy,

Ohio University, Athens, OH 45701, USA.

(Dated: May 16, 2024)

Abstract

We attempted to grow a thin film of BiN by co-deposition of bismuth and nitrogen on rock-salt structure MgO (001) substrates. Furthermore, we studied the effect of variation of the growth temperature and the nitrogen to bismuth flux ratios on sample growth. For the samples grown and conditions used, we do not find strong evidence for the formation of a bulk Bi-N alloy. Even for very high nitrogen to bismuth flux ratio, we observed only bismuth and no nitrogen using bulk Rutherford back-scattering spectroscopy measurements, and only 1-2% nitrogen was seen through surface Auger electron spectroscopy measurements. The *in-plane* lattice measurements show that the resulting Bi (110) samples are strained, which is presumably caused by lattice mismatch between the sample and the substrate when grown without any buffer layer. The use of a high-temperature buffer layer helps to release strain in the sample but only along one axis. Measurements of the atomic layer spacing using X-ray diffraction and also scanning tunneling microscopy confirm the Bi (110) thin film sample structure.

Keywords: Bismuth, Molecular beam epitaxy, Scanning tunneling microscopy

* Corresponding author: smitha2@ohio.edu

I. INTRODUCTION

In recent years, bismuth and its compounds, namely Bi_2Te_3, Bi_2Se_3, and $Bi_{1-x}Sb_x$ have emerged as an intriguing research field in the condensed matter community. These materials hold potential for applications in room temperature spintronics and quantum devices [1, 2]. While these materials behave like insulators in bulk, they exhibit metallic surface states that are topologically protected from the environmental influences [3, 4]. Topological materials, particularly Bi_2Te_3, and Bi_2Se_3, are well known for their widespread use in thermoelectric devices [5, 6].

Among various bismuth based topological insulators that have been reported, $Bi_{1-x}Sb_x$ stands out as the most promising due to its large spin Hall angle ($\sim 52\,^{\circ}$) [7], high conductivity [8], and potential for constructing low-current spin-orbit torque (SOT) magnetoresistive random-access memories (MRAM) [9, 10]. The growth of $Bi_{1-x}Sb_x$ alloy has been reported by various groups. Ueda *et al.* reported the molecular beam epitaxy (MBE) growth and characterization of $Bi_{1-x}Sb_x$ on semi-insulating GaAs (111)A substrates. They studied the conductivity of the samples by varying the Sb concentration and confirmed the existence of metallic surface states of $Bi_{1-x}Sb_x$ both inside and outside of the topological insulating region [11]. Similarly, Yao *et al.* reported the growth of BiSb thin films using MBE and investigated the role of crystal orientation and surface termination of the GaAs (111) substrates on the growth of BiSb [12]. They reported that the growth of BiSb film is not only affected by the symmetry of substrates but is also strongly affected by surface termination. More interestingly, Sadek *et al.* reported highly epitaxial growth of rhombohedral BiSb on cubic GaAs despite large mismatches and different crystalline matrices [13].

Despite extensive research on bismuth-chalcogenides and bismuth-antimony compounds, efforts to synthesize Bi-N thin films have gone largely unreported until now. Indeed, by searching the literature, we did not find any papers reporting the synthesis of Bi-N or BiN by MBE growth or other methods. We did find an article on the synthesis of bismuth-nitrogen cage compounds published recently. However, these cage compounds actually involve a complex chemical formula referenced as [Cl-Bi(μ_3-N-TMP)]$_4$- type heterocubane [14]. As both nitrogen and antimony belong to the same groups in the periodic table, we are interested in growing and studying the surface properties of thin films of bismuth-nitrogen compounds. We are particularly intrigued by the possibility of bismuth-nitrogen alloy growth and in-

vestigating whether the Bi-N alloy exhibits similar topological properties as $Bi_{1-x}Sb_x$ or not. In this study, we attempted to co-deposit multiple samples of bismuth and nitrogen on MgO(001) substrates by varying the growth parameters, such as growth temperature and bismuth to nitrogen flux ratios.

II. EXPERIMENTAL

Samples were grown in a custom-designed ultrahigh vacuum (UHV) system, which consists of an MBE chamber coupled with an analysis chamber (AC). The MBE chamber is equipped with a radio frequency (rf) plasma source for nitrogen and an effusion cell for bismuth. The AC consists of a room temperature scanning tunneling microscope (RT-STM) and Auger electron spectroscopy (AES). Prior to loading the substrates into the MBE chamber, they were cleaned with acetone followed by isopropanol in the ultrasonicator. The loaded substrates are then annealed at 1000 °C for an hour in presence of nitrogen plasma in the growth chamber. The temperature during the growth is monitored using a pyrometer, and a thermocouple situated just beneath the substrate on the growth stage. After annealing, the substrate temperature is lowered to the desired growth temperature. In this paper, we are reporting three different growth temperatures, namely: room temperature (27 °C), 150 °C, and 460 °C for co-deposition of bismuth and nitrogen. The results obtained from samples grown at different temperatures will be discussed in the following section.

The nitrogen flux during the sample growth is kept constant ($J_N = 3.5 \times 10^{14}$ atoms/ cm^2 s), while varying the bismuth flux (J_{Bi}). The nitrogen flux is determined following the GaN growth procedure reported by Smith *et al.* [15] and bismuth flux is measured using the Quartz crystal thickness monitor (QCM). The base pressure of the growth chamber for all sample growth is 10^{-9} Torr with N plasma power set at 510 Watts forward power and at 2 Watts reverse power. The co-deposition is started by deposition of bismuth from a crucible with grains of Bi (99.999 % purity) and nitrogen (99.999 % purity) from nitrogen plasma source. During the growth, sample's surface is monitored using *in-situ* reflection high energy electron diffraction (RHEED) of energy 20 keV.

Following the growth, the samples are transferred to the AC without breaking the vacuum and investigated with *in-situ* RT-STM and AES. After removal from the AC, the samples are analyzed using a RIGAKU $\theta - 2\theta$ powder X-ray diffraction (XRD) with Cu-K_α source of

wavelength 1.541 Å. Atomic force microscopy (AFM) is used to scan the sample in contact mode and the post-processing of data is done using Gwyddion software [16]. Rutherford backscattering (RBS) is used for the chemical composition determination of the samples, and fitting was performed using the RUMP simulation code[17]. The RBS data were taken using a 2.2 MeV helium ion beam from the 4.5 MV tandem accelerator in the Edwards Accelerator Laboratory of Ohio University. The beam was scattered through 168°. To avoid channeling the beam was incident at 7.5° with respect to the surface normal, and the sample was rotated about 20° with respect to the major crystal axes.

III. RESULTS AND DISCUSSION

Many samples of Bi-N alloy were grown on MgO (001) substrates at three different growth temperatures from room temperature to 460 °C with different nitrogen to bismuth flux ratios. Some of the samples were grown directly on top of substrates and some of them were grown after the growth of thin buffer layer. In this section, we will discuss the results of the Bi-N alloy grown by MBE on MgO (001) substrates at different temperatures, and different N to Bi flux ratios.

Figure 1 depicts the RHEED patterns for the MgO substrate and various grown thin films. The left panel of the figure represents the $[100]_{MgO}$ direction, while the right panel represents the $[110]_{MgO}$ direction. The RHEED patterns of the MgO substrate after 1 hour of annealing at 1000 °C are shown in Fig. 1(a). In all samples, we observed a four-fold symmetry in the RHEED pattern, similar to that of the MgO substrate. The RHEED patterns for the grown (Bi + N co-deposited) thin film samples S1, S3, and S4 are shown in Figs. 1(b,c, and d/e), respectively. In general, careful measurement of the streaks spacings shows that they decreased in both directions compared to the substrate streaks spacings. The decreased streaks spacings in the RHEED pattern implies that the grown samples have larger lattice constants than the MgO substrate.

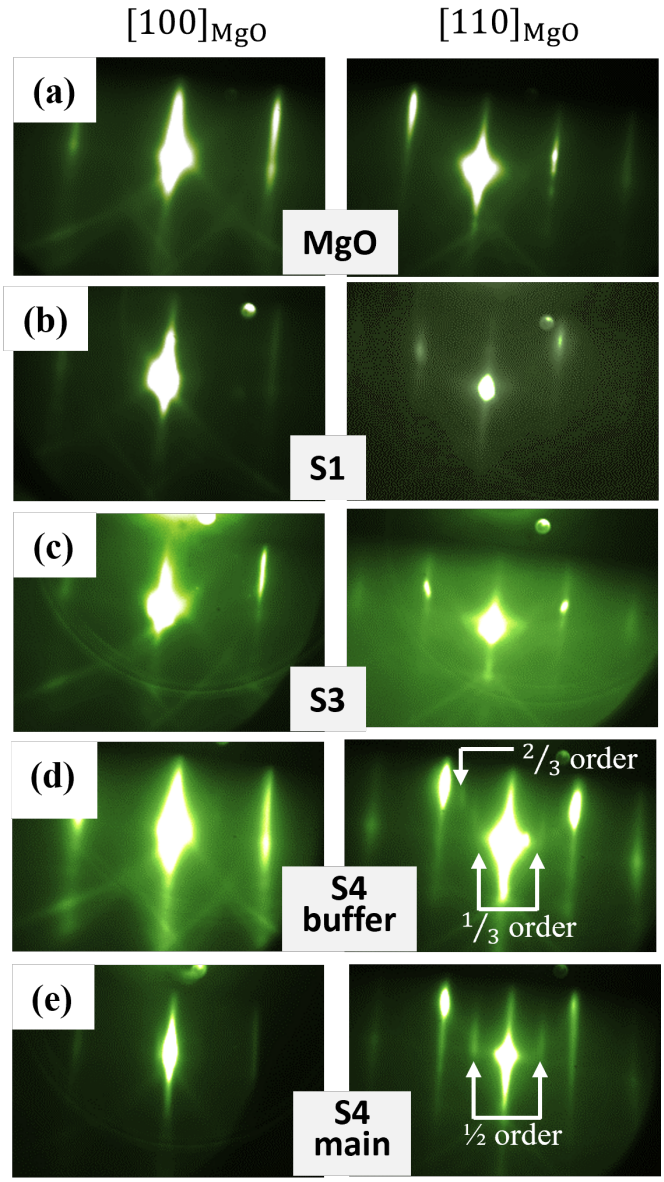

FIG. 1. RHEED patterns for substrate and samples. (a) MgO substrate at 150 °C temperature after 1 hr. of annealing at 1000 °C in presences of nitrogen plasma. (b) sample S1 grown at 150 °C. (c) post-nitridation of sample S3 grown at room temperature.(d) buffer layer growth of sample S4 grown at 460 °C. (e) main layer of sample S4 grown at 150 °C. The circular spot observed in (b), (c) and (d) near primary streak is likely caused by an artifact that is unrelated to the surface characteristics being studied.

The stoichiometry of thin films is determined using *in-situ* AES. The AES system uses 5 keV electrons hitting the sample at normal incidence to acquire AES spectra. In AES measurement, ratio of Bi and N is calculated based on the relation Bi:N = $(I^{pp}_{Bi}/S_{Bi})/(I^{pp}_{N}/S_{N})$,

where I_{Bi}^{pp} and I_{N}^{pp} are the peak to peak intensities in dN(E)/dE vs energy curve for Bi105 and N389 respectively. The S_{Bi} and S_N represent the sensitivity factor of Bi105 and N389, with values of 1.1306 for Bi105 and 0.9157 for N389 [18]. The AES spectra for samples S1 and S4 are shown in Fig. 2(a). For each sample, the position of Bi105, Bi132, and N389 peaks is denoted by a black triangle, orange circle, and purple square, respectively. The green curve in Fig. 2(a) corresponds to the AES spectra for sample S1. We observed a significant bismuth signal at 105 eV, while the nitrogen signal at 389 eV was minimal. The bismuth-to-nitrogen ratio calculation, from AES spectra, revealed that $\sim 98\%$ of chemical composition in the film surface layers is bismuth. The very small amount of nitrogen seen in the AES spectrum is attributed to nitrogen adsorption rather than bulk N incorporation.

Further evidence for the chemical composition of the grown films is obtained from RBS, which has been performed for samples using a helium ion beam of incident energy of 2.2 MeV and a backscattering angle of 168°. The plot showing the RBS spectrum for grown sample S1 as a function of energy is presented in Fig. 2(b). The black and red lines indicate the experimental and simulated graphs, respectively. In our RBS data for sample S1, we have no evidence for a nitrogen peak or step but only a bismuth peak. The oxygen step comes just after the magnesium step due to the MgO substrate. From the RBS plot, the bismuth peak is observed at 2.04 MeV (channel 312). The substrate edges for magnesium and oxygen are observed at 1.14 MeV and 0.80 MeV, respectively. If there was any nitrogen present, it would be seen at 0.69 MeV. The expected position for nitrogen in the spectrum is indicated by red arrow in the inset of Fig. 2(b). Although a small amount of nitrogen was observed in AES, RBS did not detect any nitrogen content in the film. So, we cannot easily conclude the existence of significant amounts of nitrogen within the bulk of sample S1. These results suggest only the presence of a thin layer of nitrogen solely on the surface of the film which can happen due to adsorption of nitrogen on a clean bismuth film surface.

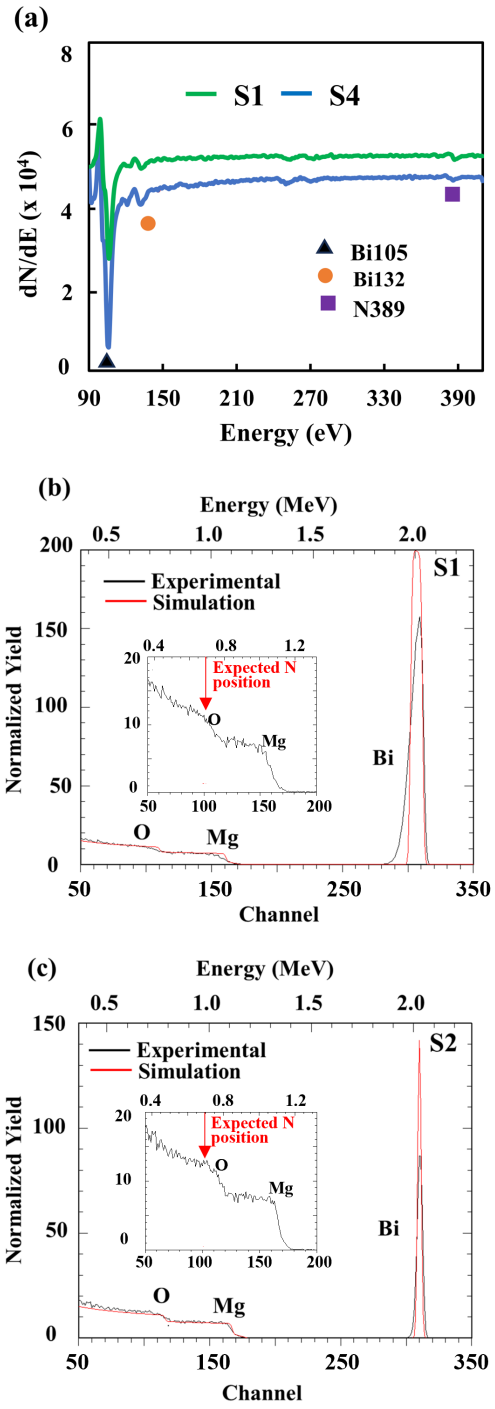

FIG. 2. (a) The AES spectra for different samples showing the positions of the Bi105, Bi132, and N389 peaks, represented by a black triangle, orange circle, and purple square, respectively. (b) The RBS plot for sample S1 showing the experimental and simulated data. (c) The RBS plot for sample S2 showing the experimental and simulated data. The inset in (b) and (c) represent the zoom-in view of spectrum from channel 50 to 200.

As can be seen from Fig. 1, the RHEED patterns of the grown samples are similar to those of the MgO (001) substrate, suggesting the growth of pseudo-cubic bismuth (100) [equivalently, rhombohedral Bi (110)]. We can calculate the corresponding *in-plane* lattice constants for the grown thin films by comparing the streaks spacings. Since the streaks spacing is proportional to the reciprocal lattice constant (a*), the *in-plane* lattice constant for the grown samples can be given by $a_S = a_{MgO}(w_{MgO}/w_S)$ [19], where a_{MgO} and a_S represent the *in-plane* lattice constants and where w_{MgO} and w_S represent the streaks spacings between first-order streaks for MgO and the grown thin films, respectively. The streaks spacings are calculated from the line profiles of the corresponding RHEED images.

Sample S1 was grown to a thickness of 262 nm at growth temperature T_S = 150 °C with a N to Bi flux ratio of 1.75 for 70 minutes (growth rate ∼ 3.743 nm/min). From the RHEED pattern for sample S1 shown in Fig. 1(b, left panel), we can clearly observe streak-point features, indicating that the surface of the sample is not very smooth. Based on the streaks spacing for the $[100]_{MgO}$ azimuth, the calculated *in-plane* pseudo-cubic lattice parameter for sample S1 is $a = 4.25 \pm 0.03$ Å. This value is smaller by 6.4 %, but comparable to, the lattice constant of bismuth metal, $a = 4.54$ Å ($a = a_{hex,Bi}$ for bulk rhombohedral Bi).[20] Also, pseudo-cubic is not really cubic, and from the $[110]_{MgO}$ RHEED streaks spacings, we calculate $b = 4.34$ Å $\pm$ 0.04 Å, which may be compared with the $b = 4.75$ Å ($b = a_{rh,Bi}$ for bulk rhombohedral Bi), a deviation of -8.6 %.

We note that the observed lattice parameters are in between the values for Bi (110) and MgO (001) *in-plane* lattice constants. This suggests that lattice-mismatch-induced (compressive) strain could be the cause and is developed in sample S1. Defining strain as

$$S = \frac{a_{observed} - a_{expected}}{a_{expected}} \times 100\%, \tag{1}$$

the S = -6.4 % along $[100]_{MgO}$ may be attributed to the 7.8 % lattice mismatch between bismuth and MgO ($a_{MgO} = 4.213$ Å) [21]. Similarly, the S = -8.6 % strain along the $[110]_{MgO}$ azimuth may be attributed to the 12.7 % mismatch with MgO.

Keeping the growth temperature constant, we increased the nitrogen to bismuth flux ratio to 7.1:1.0 for sample S2, aiming to decrease the amount of bismuth and increase nitrogen content in the film. However, despite the increased N:Bi flux ratio compared to sample S1, we observed very small change to the results, namely a similar RHEED pattern (not shown here) with a similar lattice constant $a = 4.27 \pm 0.04$ Å along $[100]_{MgO}$ for S2 of

thickness $\sim$ 84 nm. The sample was grown at slower rate of 0.933 nm/min. The calculated lattice constant suggests that the grown sample S2 is also strained to the MgO substrate. The chemical composition of sample S2 was also determined by RBS, which shows uniform growth of bismuth with no nitrogen content as shown in Fig. 2(c). If there was any significant nitrogen content in the bulk film, we would expect to see a nitrogen peak in the RBS. From the inset in Fig. 2(c), we can clearly see only Mg and O peak. This tells us that there is not any nitrogen, or very little, within the sample. As seen in Fig. 2(c), the substrate peak appears to be stronger for sample S2 than sample S1, which is due to the lower thickness of sample S2.

Since we did not observe significant effects of a higher N:Bi flux ratio in the growth of sample S2, we drastically increased the flux ratio (J_N/J_{Bi}) to 25.0:1.0. We also decreased the growth temperature to $T_S = 27$ °C (room temperature) for sample S3. In addition, after the growth of the 21 nm thick sample S3 at the growth rate of 0.28 nm/min, we further nitridated the film at room temperature for an additional 100 minutes. The RHEED patterns for sample S3 after nitridation are shown in Fig. 1(c). The RHEED still shows very similar streaks patterns to what we observed for other previous samples. Additionally, for sample S3, the RHEED along the $[110]_{MgO}$] has a streak-point pattern similar to that observed in sample S1 along $[110]_{MgO}$. The calculated *in-plane* lattice constant for sample S3 is a= 4.16 $\pm$ 0.03 Å with -8.37 % strain in the sample along $[100]_{MgO}$ direction. Similarly, from $[110]_{MgO}$ direction, the calculated lattice parameter is $b = 4.18 \pm 0.04$ Å with -12.0 % strain. The calculated a value of sample S3 is 2.12 % smaller than that of sample S1, and 2.58 % smaller than that of sample S2; while the b value of sample S3 is 3.69 % smaller than that of S1. The smaller lattice constant and higher strain in the sample is attributed to it being much thinner compared to sample S1. Usually, to release the strain from the grown thin film sample, it is necessary to grow a thicker sample. The decrease in strain with increase in sample thickness has been reported in MBE-grown β-In_2Se_3 and Bi_2Se_3 samples [22].

The direct co-deposition of Bi and N on top of the MgO substrate did not help to achieve Bi-N alloy, as discussed in the previous sections. Therefore, we followed a two-step process to grow sample S4. The first step involved the co-deposition of bismuth and nitrogen to form a buffer layer (S4B) at $T_S = 460$ °C with J_N:J_{Bi} = 25.0:1.0 maintaining the growth rate of 0.28 nm/min. The expected thickness of the buffer layer is nearly 17 nm. After the buffer layer growth, the main layer (S4M) also of thickness $\sim$ 17 nm was grown at $T_S = 150$

°C while maintaining the same flux ratio and keeping the same growth rate. Both S4B and S4M were grown for an hour. So, the total thickness of sample S4B+S4M is 34 nm. Fig. 1(d) shows the RHEED patterns of S4B. The RHEED pattern along the $[100]_{MgO}$ direction appears identical to the samples discussed in previous sections. However, faint one-third order streaks are observed along the $[110]_{MgO}$ direction. The position of fractional streaks is indicated in the figure. Based on the RHEED line profiles, the *in-plane* lattice constants of S4B are determined to be $a = 4.31 \pm 0.05$ Å and $b = 4.18 \pm 0.06$ Å along $[100]_{MgO}$ and $[110]_{MgO}$ direction, respectively. As the calculated lattice parameters are smaller for sample S1, S2, S3, and S4B compared to Bi (110), where we expect to see 4.54 Å × 4.75 Å [23] [see fig. 5(a)], it implies our samples are under compression caused by substrate strain, which seems likely since the measured values are so close to the value for MgO (4.213 Å).[21]

Regarding the strain versus thickness and sample temperature, the samples S1, S2, and S4B show remarkably similar lattice constants (a) despite vastly different thicknesses. But for sample S3 we see a value of 4.16 ± 0.03 Å, less than the MgO lattice constant, for room temperature co-deposition. One possibility is that this could be explained by a Bi-N alloy having a smaller lattice constant. Further experiments are needed to explore this further.

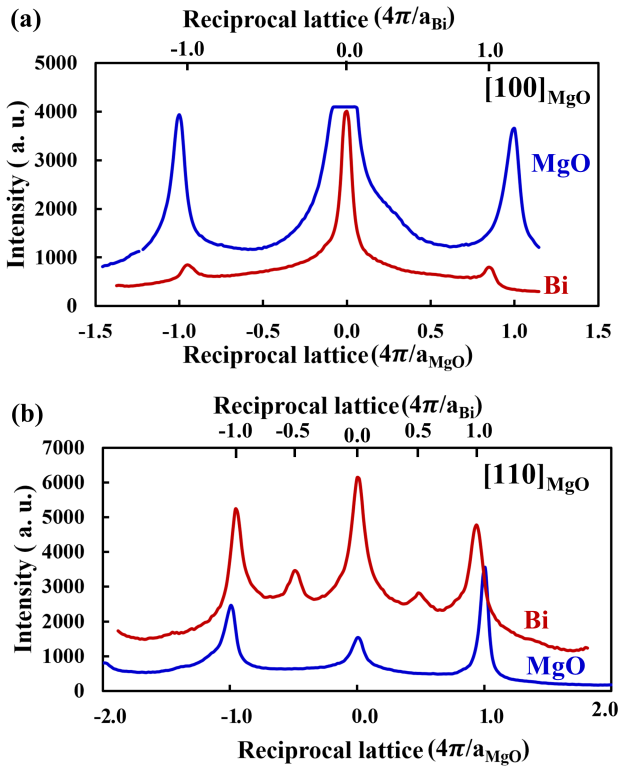

FIG. 3. RHEED line profiles for sample S4M and MgO substrate along two directions: (a) $[100]_{MgO}$ direction (b) $[110]_{MgO}$ direction.

RHEED patterns of S4M are shown in Fig. 1(e), and the corresponding line profiles are shown in Fig. 3. Along both directions, the patterns are streakier, and streaks spacings are narrower compared to the MgO substrate. Moreover, one-third order fractional streaks converted to the half-order fractional streaks along [110], and appear to be more pronounced. The lattice constants for sample S4M are found to be $a = 4.64 \pm 0.04$ Å, and $b = 4.29 \pm 0.05$ Å. Therefore, the a value of S4M is mostly relaxed while the b value remains strained compared to bulk Bi (110) structure. As the (110) notation is rhombohedral notation and is equivalent to a $(10\bar{1}2)$ hexagonal notation [20], the surface lattice should correspond to a rectangular lattice. Despite having nearly the same film thickness as sample S3 and being much thinner than sample S1 (see Table II), the surface strain has been significantly reduced along the a-direction but not along the b-direction. This suggests that the growth of the S4B layer aids in the relaxation of the S4M layer, even at lower sample thicknesses. The *in-plane* lattice parameters calculated from RHEED are summarized in Table I.

TABLE I. The calculated strained *in-plane* lattice parameters of various Bi(110) samples.

Sample	a (Å)	b (Å)	Strain along a	Strain along b
S1	4.25 ± 0.03	4.34 ± 0.04	-6.39 %	-8.63 %
S2	4.27 ± 0.04	N/A	-5.95 %	N/A
S3	4.16 ± 0.03	4.18 ± 0.04	-8.37 %	-12.0 %
S4B	4.31 ± 0.03	4.18 ± 0.06	-5.07 %	-12.0 %
S4M	4.64 ± 0.04	4.29 ± 0.05	2.20 %	-9.68 %

We further carried out the AES measurements on sample S4 to confirm the chemical composition of the film. As depicted by the blue curve in Fig. 2, there is minimal or no nitrogen peak observed at an energy of 389 eV, while a strong bismuth peak is present at 105 eV. AES measurements show that only $\sim$ 1 % of nitrogen is present in the film. Although 1% nitrogen was seen in AES at the surface, the film is more relaxed compared to other films which does not necessarily imply nitrogen incorporation in the bulk film. Based on both RHEED and AES measurements, we can confidently conclude that sample S4M consists of bismuth with only a small amount of nitrogen at the surface.

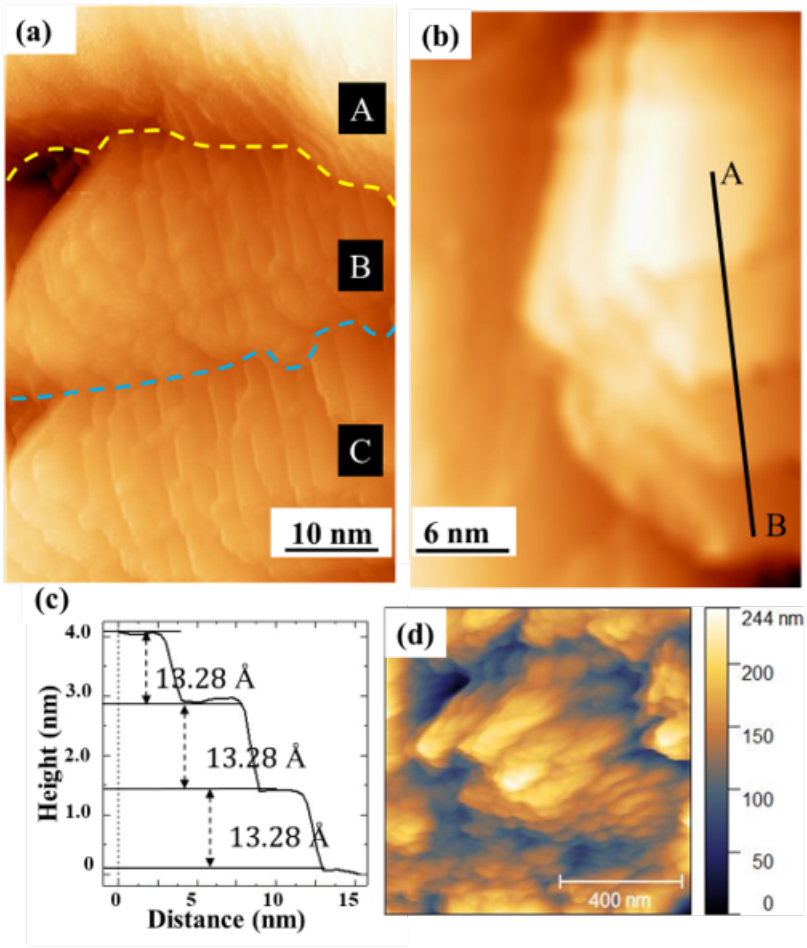

FIG. 4. (a) 42 nm × 62 nm topographic STM image showing general features of the sample S1. (b) 25 nm × 37 nm topographic STM image of sample S1 showing four terraces. (c) Line profile across the terraces corresponding to the line AB shown in (b). (d) 1 μm × 1 μm topographic AFM image of sample S1.

RT-STM is used to examine the surface of sample S1. The STM images are taken in constant current mode using a sharp tungsten tip to scan the surfaces. The STM image of sample S1 is illustrated in Fig. 4. Fig. 4(a) shows a topographic STM image of 42 nm × 62 nm of the bismuth surface, which reveals general surface characteristics. The surface exhibits a multi-terrace and step-edge-like structure with a deep valley. Furthermore, three distinct mounds, labeled as A, B, and C, are visible. The borders between the mounds are indicated by the yellow and blue dotted curves. Mound A has a steeper slope and a rough surface, while mound B and mound C have smooth surfaces with several small terraces.

Fig. 4(b) shows a topographic STM image of 25 nm × 37 nm of the same sample,

acquired by repositioning the tip. The image reveals four atomically smooth terraces with steps. In order to measure the step height of each terrace, a line profile is drawn along line AB in the STM image, as shown in Fig. 4(b), and the corresponding line profile is presented in Fig. 4(c). The average height of each step is determined to be 13.3 ± 0.1 Å. The height difference of 13.3 ± 0.1 Å for the steps is in good agreement with the 4× 3.28 Å [the single layer spacing for Bi(110)] observed on different substrates [23, 24]. Furthermore, the observed four layers of bismuth stacking are clearly visible in the crystal model shown in Fig. 5(b), and consistent with the optimized Bi(110) model presented by Nagao *et al.* for thin layer of Bi(110). The main difference between our sample and that of Nagao *et al.* is the thickness of the grown sample. They observed Bi(110) pseudocubic structure up to 6 ML of bismuth growth while we observe pseudocubic structure for considerably thicker samples like S1. This could be due to the sample being strained to the MgO substrate. Although we do not have an atomic resolution STM image for these samples, the lattice constants calculated from the RHEED patterns are consistent with the rectangular surface lattice parameters observed by Nagao *et al* [23]. Similar even-number stacking of the Bi (110) surface layers grown on a variety of substrates have been reported, such as on Si(111)-7×7 [23], Ge (111)-c(2×8) [25], Si(111)-$\sqrt{3} \times \sqrt{3}$B [26] and on highly ordered pyrolytic graphite (HOPG) [27].

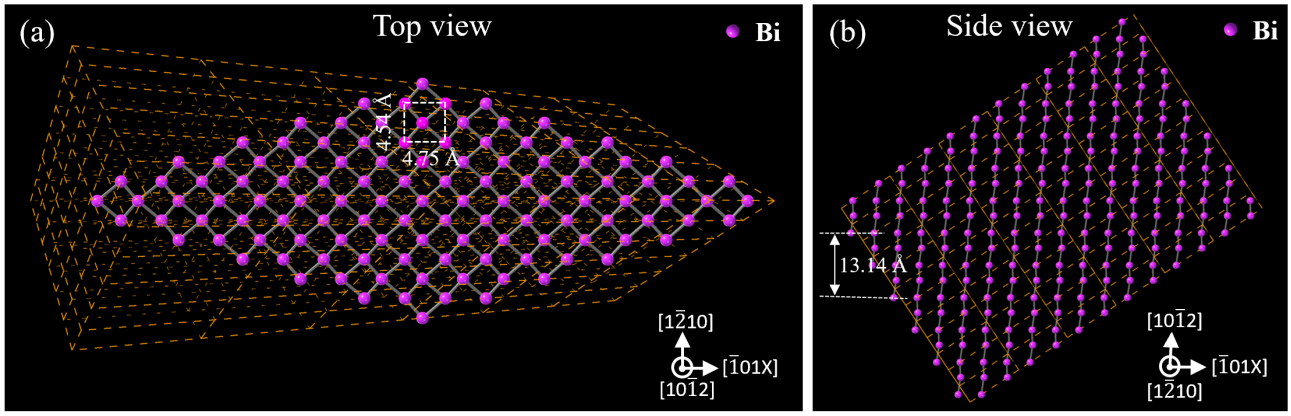

FIG. 5. Crystal structure for Bi (110): (a) *in-plane* orientation (b) *out-of-plane* orientation. The directions are shown in hexagonal crystal notation and X ≈ 4.531. This irrational value equals 4655/1025 and comes from the Miller indices [-1025 0 1025 4655]. Also note that the lattice parameters shown in the model are bulk values, not the values for the measured samples. See Table 1 for measured values. The epitaxial relationship of the measured Bi samples to MgO can be written in hexagonal (for Bi) and cubic (for MgO) notation as $[\bar{1}01X]_{Bi} \parallel [100]_{MgO}$, $[1\bar{2}10]_{Bi} \parallel [010]_{MgO}$, and $[10\bar{1}2]_{Bi} \parallel [001]_{MgO}$.

Fig. 4(d) shows a 1 μm×1 μm AFM image of sample S1 with root mean square (RMS) surface roughness of 34 nm. The image reveals large mounds with multiple layers. Additionally, the AFM image exhibits a steeper surface, resembling the mound A observed in the STM image. The presence of multiple mounds and the rougher surface observed in the STM and AFM images are consistent with the non-streaky RHEED pattern shown in Fig. 1(b).

Figure 6 displays the AFM images of sample S4. The large size, of 1 μm×1 μm, AFM image of surface roughness 15 nm is shown in Fig. 6(a). Randomly-oriented islands of varying size and deeper valleys can be seen in the figure. Some islands exhibit layer-by-layer stacking of three or more layers, as shown in Fig. 6(a) and (d). The sample also exhibits long and flatter terraces as shown in Fig. 6(b). The surface roughness of the region shown in Fig. 6(b) is only 2.2 nm, which indicates the much smoother region of the film. The lower roughness of the sample is consistent with the streaky RHEED patterns as shown in Fig. 1(e). Furthermore, Fig. 6(c) presents a 3D view of Fig. 6(b), revealing clear steps and terraces forming a staircase structure where we can see the stacking of four flat terraces.

Similar terraces of bismuth can also be observed in the STM image of sample S1 in Fig. 4.

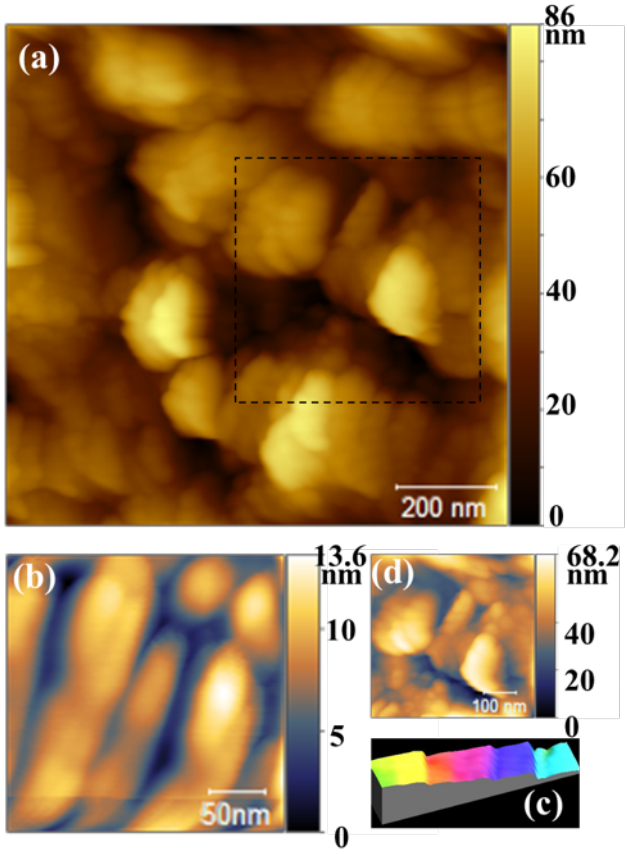

FIG. 6. AFM image of sample S4 acquired at RT. (a)1 μm×1 μm AFM image showing multiple islands. (b) 250 nm×250 nm AFM image showing flatter region. (c) 3D view of (b) showing the "staircase" structure. (d) 0.5 μm×0.5μm AFM image of black boxed region in (a).

After removing the samples from the UHV chamber, the crystal orientation is analyzed using XRD. Figure 7 displays the XRD spectra for samples S1, S2, and S4. For all samples, the peak positions are identified using CrystalDiffract® software and converted to rhombohedral notation from hexagonal notation. The conversion from the hexagonal to rhombohedral notation is discussed in reference [20]. As observed in Fig. 7, the most prominent and intense peak for all samples is observed at 42.9°, corresponding to a d value of 2.11 ± 0.01 Å, indicating the MgO 002 peak. Fig. 7(a) shows the XRD pattern for sample S1. The second most intense peak for this sample is observed at 27.2°, which corresponds to Bi 110. The presence of an intense Bi 110 peak, with d value of 3.28 ± 0.01 Å suggests that a significant portion of the sample surface is composed of Bi (110). Additional small peaks of bismuth

are also observed and labeled in the figure, while no other peaks corresponding to Bi-N alloy are detected. At 22.4°, a small Bi 111 peak is observed, giving a d value of 3.97 ± 0.03 Å. The calculated spacing corresponds to the interplanar distance on the surface of Bi (111) (3.94 Å) [20, 23]. Other small peaks seen in the XRD pattern are: Bi 112 at 37.9°, Bi $10\bar{1}$ at 39.6°, Bi 222 at 45.9°, and Bi 002 at 48.6°. Although XRD shows multiple minority phases whereas RHEED indicates essentially one single phase, it is understood that RHEED only sees the surface while XRD senses the bulk of the film. It can also be that the RHEED beam illuminates only a thin layer of the sample surface, while the XRD beam illuminates a larger area. It can also be a matter of the intensity being too small and/or the azimuthal angle not being correct for seeing the peaks from these minority phases. As all the peaks observed in our data correspond to bismuth peak, it can be concluded that an alloy of bismuth and nitrogen is not formed in the sample.

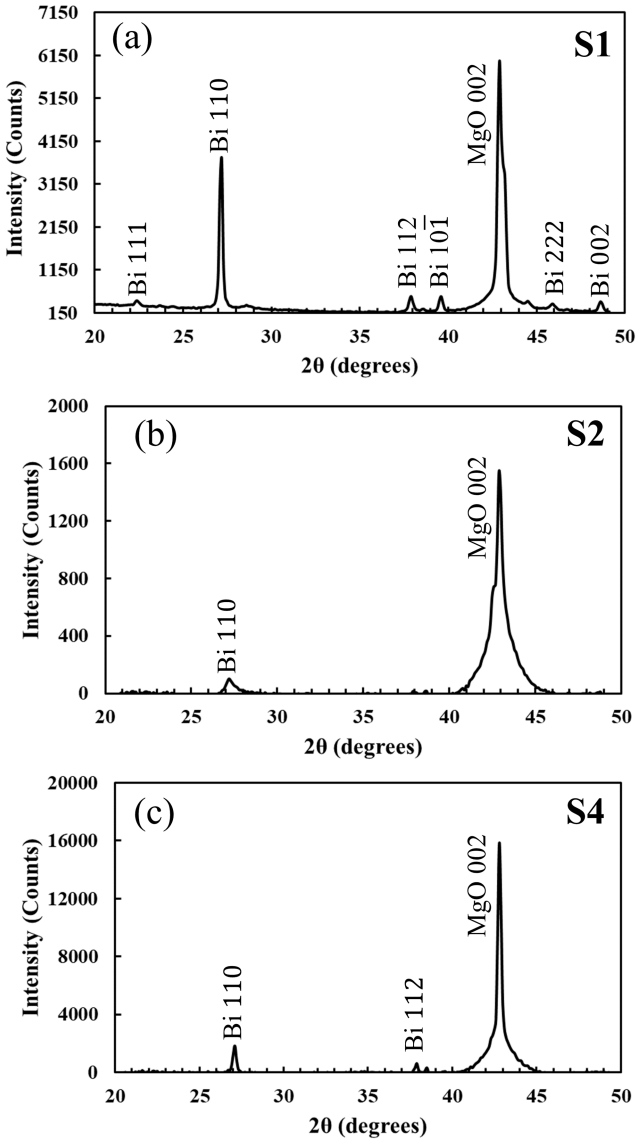

FIG. 7. XRD spectra for co-deposited Bi-N samples on MgO (001) substrate showing different peak positions; (a) sample S1 (b) sample S2 (c) sample S4. Peaks are denoted in rhombohedral notation.

As depicted in Fig. 7(b), representing the XRD spectra for sample S2, only two peaks are observed: MgO 002 and Bi 110. In contrast to sample S1, no other small peaks are detected. Similarly, the XRD pattern for sample S4, shown in Fig. 7(c), also exhibits solely bismuth peaks. At 27.0°, Bi 110 is seen, along with a tiny Bi 112 peak at 38.0°. None of the samples exhibit peaks other than the bismuth peaks in the XRD patterns, indicating that the grown samples purely consist of bismuth. Moreover, our *out-of-plane* values measured

from XRD range from 3.28 Å to 3.30 Å, in excellent agreement with the 3.29 Å average layer spacing expected for bulk Bi (110). Therefore, this is consistent with lack of nitrogen within the bismuth film instead of either a contraction or an expansion caused by nitrogen for this Bi (110) structure. Based on XRD, RHEED, and STM results, in rhombohedral notation for bismuth and cubic notation for MgO, the substrate-sample epitaxial relationship is found to be $[1\bar{1}0]_{Bi} \parallel [010]_{MgO}$, and $[110]_{Bi} \parallel [001]_{MgO}$. In terms of hexagonal notation for bismuth with cubic notation for MgO, the epitaxial relationship can be written as $[\bar{1}01\mathrm{X}]_{Bi} \parallel [100]_{MgO}$, $[1\bar{2}10]_{Bi} \parallel [010]_{MgO}$, and $[10\bar{1}2]_{Bi} \parallel [001]_{MgO}$.

From the various *in-situ* and *ex-situ* measurements it is clear that we do not observe, after Bi-N co-deposition, nitrogen incorporation in the film. But we do observe a structure consistent with a Bi (110) 'pseudo-cubic' model described in several references [20, 23, 28]. The key difference is that the Bi (110) structure we observe is strained to the underlying substrate even for thicker samples. The compressed lattice constant even for the very thick film sample S1 ($\sim$ 262 nm) does not imply lattice contraction caused by nitrogen incorporation within the film. We have recent experience with metallic Mn_3Sn thin films on *c*-plane sapphire substrates in which strains similar to those seen here were observed to very large film thickness [29]. Table II summarizes the growth parameters, the film thickness, and the ratio of bismuth to nitrogen content in the various samples discussed here.

TABLE II. Summary of growth parameters, growth rate, sample thickness, and ratio of bismuth to nitrogen observed from AES for different samples grown on MgO (001) substrates.

Sample	Growth temperature (°C)	J_N/J_{Bi}	Growth rate (nm/min)	Expected thickness (nm)	Bi:N
S1	150	1.75	3.743	$\sim$ 262	1:0.02
S2	150	7.14	0.933	$\sim$ 84	N/A
S3	27	25.0	0.281	$\sim$ 21	N/A
S4B	460	25.0	0.283	$\sim$ 17	N/A
S4M	150	25.0	0.283	$\sim$ 17	1:0.01

IV. CONCLUSIONS AND FUTURE WORK

The co-deposition of Bi-N on MgO (001) substrates by MBE was studied using RHEED, STM, XRD, AES, and RBS. Careful measurement from various *in-situ* and *ex-situ* techniques reveal that bismuth and nitrogen do not react to form a crystalline compound similar to the case of bismuth and antimony in the conditions used, despite that both antimony and nitrogen belong to the same group in the periodic table. Our current work demonstrates that, under the conditions of N-rich growth and low- to mid-range substrate growth temperatures used, the formation of a bismuth-nitrogen alloy is not feasible.

On the other hand, we discovered the formation of (110)-oriented Bi thin films on MgO (001) substrates. This is very clear from the XRD patterns revealing the 110-oriented (rhombohedral notation) Bi thin film structure. The detailed lattice parameters were found to be almost independent of the Bi:N flux ratio, once again indicating that nitrogen incorporation into the films did not happen. For all the resulting Bi (110) samples, we observed *in-plane* strain caused by lattice mismatch with the MgO substrate. The *in-plane* strain was partially released after depositing onto a high-temperature bismuth buffer layer. The STM images revealed macrosteps equal in height to 4 Bi (110) layers.

Although not confirming bulk BiN structures, our results do suggest surface layers containing nitrogen. And we cannot rule out the formation of Bi-N bonding at the surface. In order to further investigate the formation of Bi-N surface alloys, we plan to use density functional theory to construct a Bi-N surface structure and analyze the possible stability and electronic properties. If possible, we will explore this structure with STM in the future.

ACKNOWLEDGMENTS

The authors acknowledge support from the U.S. Department of Energy, Office of Basic Energy Sciences, Division of Materials Sciences and Engineering under Award No. DE-FG02-06ER46317. The authors would like to thank Dr. Eric Stinaff and his students for titanium back-coating on substrates, and Dr. Savas Kaya for allowing to use the AFM in his lab.

AUTHOR DECLARATIONS

Conflict of Interest

The authors have no conflicts to disclose.

DATA AVAILABILITY

The data supporting this study's findings are openly available in Zenodo at [Link will be added later].

---

[1] M. Z. Hasan, and C. L. Kane, Rev. Mod. Phys. **82**, 3045 (2010).

[2] P. Ghaemi, R. S. K. Mong, and J. E. Moore, Phys. Rev. Lett. **105**, 166603 (2010).

[3] H. Zhang, C. Liu, X. Qi, X. Dai, Z. Fang, and S. Zhang, Nat. Phys. **5**, 438 (2009).

[4] Y. Xia, L. Wray, D. Qian, D. Hsieh, A. Pal, H. Lin, A. Bansil, D. Grauer, Y. S. Hor, R. J. Cava, and M. Z. Hasan, Nat. Phys. **5**, 398 (2009).

[5] H. Cao, R. Venkatasubramanian, C. Liu, J. Pierce, H. Yang, M. Z. Hasan, Y. Wu, and Y. P. Chen, Appl. Phys. Lett. **101**, 162104 (2012).

[6] H. Linda, S. Linda, and U. H*ä*ussermann, Phys. Rev. B **72**, 184101 (2005).

[7] N. H. D. Khang, Y. Ueda, and P. N. Hai, Nat. Matter. **17**, 808-813 (2018).

[8] D.-X. Qu, S. K. Roberts, and G. F. Chapline, Phys. Rev. Lett. **111**, 176801 (2013).

[9] N. H. D. Khang, S. Nakano, T. Shirokura, Y. Miyamoto, and P. N. Hai, Sci. Rep. **10**, 12185 (2020).

[10] S. Fukami, T. Anekawa, C. Zhang,and H. Ohno, Nature Nanotech. **11**, 621-625 (2016).

[11] Y. Ueda, N. H. D. Khang, K. Yao, and P. N. Hai, Appl. Phys. Lett. **110**, 062401 (2017).

[12] K. Yao, N. H. D. Khang, and P. N. Hai, J. Crystal Growth **511**, 99-105 (2019).

[13] D. Sadek, D. S. Dhungana, R. Coratger, C. Durand, A. Proietti, Q. Gravelier, B. Reig, E. Daran, P. F. Fazzini, Fuccio Cristiano, A. Arnoult, and S. R. Plissard, ACS Appl. Mater. Interfaces **13**, 36492−36498 (2021).

[14] A. Schulz, M. Thomas, and A. Villinger, Inorg. Chem. **59**, 3344 (2020).

[15] A. R. Smith, R. M. Feenstra, D. W. Greve, J. Neugebauer, and J. E. Northrup, Appl. Phys. A **66**, S974 (1998).

[16] D. Nečas, P. Klapetek, Cent. Eur. J. Phys. **10(1)**, 181 (2012).

[17] L. R. Doolittle, Nucl. Inst. Meth. **B9**, 334 (1985).

[18] K. D. Childs, B. A. Carlson, L. A. LaVanier, J. F. Moulder, D. F. Paul, W. F. Stickle, and D. G. Watson, *Handbook of Auger Electron Spectroscopy*, Physical Electronics Industries, Minnesota, (1995), p. 391-392.

[19] J. E. Mahan, K. E. Geib, G. Y. Robinson, and R. G. Long, J. Vac. Sci. Technol. A **8**, 3692 (1990).

[20] P. Hofmann, Progress in Surface Science **81**, 191-245 (2006).

[21] H. Yang, H. Al-Brithen, E. Trifan, D. C. Ingram, and A. R. Smith, J. Appl. Phys. **91**, 1053 (2002).

[22] Q. Li, Y. Wang, T. Li, W. Li, F. Wang, A. Janotti, S. Law, and T. Gu, ACS Omega **5(14)**, 7738-7744 (2020).

[23] T. Nagao, J. T. Sadowski, M. Saito, S. Yaginuma, Y. Fujikawa, T. Kogure, T. Ohno, Y. Hasegawa, S. Hasegawa, and T. Sakurai, Phys. Rev. Lett **93**, 105501 (2004).

[24] G. Bian, X. Wang, T. Miller, T. C. Chiang, P. J. Kowalczyk, O. Mahapatra, and S. A. Brown, Phys. Rev. B **90**, 195409 (2014).

[25] S. Hatta, Y. Ohtsubo, S. Miyamoto, H. Okuyama, and T. Aruga, App. Surf. Sci. **256**, 1252 (2009).

[26] K. Nagase, R. Ushioda, K. Nakatsuji, T. Shirasawa, and H. Hirayama, Appl. Phys. Exp. **13**, 085506 (2020).

[27] S. A. Scoot, M.V. Kral, S.A. Brown, Surf. Sci. **587**, 175 (2005).

[28] H. Hirayama, Advances in Physics: X **6**, 1845975 (2021).

[29] S. Upadhya, T. Erickson, H. Hall, A. Shrestha, D. C. Ingram, K. Sun, J. C. M. Hernandez, G. H. Cocoletzi, N. Takeuchi, and A. R. Smith, J. Vac. Sci. Technol. A **41**, 042710 (2023).